Capillary pressure at irregularly shaped pore throat

H.S. Suh & D.H. Kang
Department of Civil and Environmental Engineering, Yonsei University, Korea

J. Jang
Department of Civil and Environmental Engineering, Hanyang University, Korea

K.Y. Kim
Korea Institute of Civil Engineering and Building technology, Goyang, Korea

T.S. Yun
Department of Civil and Environmental Engineering, Yonsei University, Korea

ABSTRACT: The capillary pressure of immiscible fluids through permeable media is determined by size and shape of pore channel. Irregular pore shape in the natural soil or rock formation however makes the accurate estimation of capillary pressure challenging. This study utilizes 3D X-ray computed tomographic imaging technology to capture the geometric features of authentic pores. We then suggest a new morphological analysis to correlate the capillary pressure at irregular pore channel with the pore shape with the aid of Lattice Boltzmann (LB) simulation. The results show that the geometry-based shape parameters of pore throats are strongly correlated with capillary pressure obtained by LB simulation, and capillary pressure at irregularly shaped pore throat is lower than that conventionally computed for inscribed circles by Young-Laplace equation. The water retention curves by adopting the morphological analysis and its correlative scheme are well consistent with experimental data. The suggested methods and results are relevant to other pore-scale processes such as geological CO_2 sequestration, methane ebullition from wetlands, and enhanced carbon recovery.

1 INTRODUCTION

The capillary pressure dominates the immiscible fluid flow through porous media under low capillary number conditions (e.g., water flow in unsaturated soils), which is primarily determined by the size and shape of pore throat as well as interfacial tension. The invading fluid is subjected to the maximum force at the point where the flow channel is the narrowest whereas the irregularity of pore throat shape hampers the accurate measurement of the capillary pressure. The Mayer and Stowe-Princen (MS-P) method can be used to analytically determine the capillary pressure based on energy balance formulated by arc menisci configurations (Mayer and Stowe, 1965; Princen, 1969a, 1969b, 1970), however, it can only be applied into capillary tubes with relatively simple cross-sections that are mathematically expressible (Mason and Morrow, 1991; Dong and Chatzis, 1995; Lago and Araujo, 2001). Lechman and Lu (2008) derivated the boundary value problem for the water lens between particles by using free energy minimization, and Likos and Lu (2004) analytically investigated the hysteresis of water retention characteristics, but they can only be implemented into spherical particle assmblies. The commonly approachable method is to extract the fitting circle which inscribes the pore throat and to compute capillary pressure using Young-Laplace equation. The method is widely used for modeling pores into a network, however, pore network model that adopts the method does not represent irregular pores and tends to overestimate the capillary pressure (Yang et al., 2015).

Pore network models are widely used to simulate multiphase fluid flow by simplifying complex pore sturucture into a network comprised of pore chambers interconnected by pore throats (Blunt, 2001; Joekar-Niasar and Hassanizadeh, 2012). The iterative computation of sustained capillary pressure across the fluid interface in a pore network can construct water retention curves, which reflects the saturation dependent water-retaining capacity of the target porous media. Again, its main problem is that either topologically realistic pore networks extracted from 3D images (Silin and Patzek, 2006; Dong and Blunt, 2009) or synthetically generated lattice-structured networks (Raoof et al., 2013; Jang and Santamarina, 2014) still represent pore throats as simple shapes. It is well known that 3D X-ray CT enables the quantification of pore structure (Wilson et al., 2012), and that by directly performing the lattice Boltzmann (LB) simulation on the 3D image enables one to accurately compute the capillary pressure at any geometry (Ramstad et al., 2009), however, the expensive computational effort and complicated governing equations often hamper the applicability. Therefore, it is desired to scrutinize

how the irregular pore shape is correlated with the actual capillary pressure acting at irregularly shaped pore throat and propose the reliable and adoptable relation that can be implemented into the pore network model.

This study acquired cross-sectional images of real pore throats during network extraction procedure from 3D X-ray computed tomographic image. LB simulation then obtained the capillary pressure and the morphological features of equilibrated non-wetting fluid at irregularly shaped pore throat. We implement simple morphological analysis technique to correlate the capillary pressure with the effective shape of pore throat. Conventional pore network simulation was then conducted in combination with the morphological technique, followed by validation process with experimental data from the literatures.

2 MATERIALS AND METHODS

2.1 *Pore network extraction and acquisition of pore throat geometries*

Two natural sands: Jumunjin sand (D_{50} = 0.59 mm, $C_u = D_{60}/D_{10}$ = 1.45, Here, D_X is the particle diameter representing that X% of total particles is smaller than D_X) and Toyoura sand (D_{50} = 0.25 mm, C_u = 1.49) are individually packed in a glass cylinder with the diameter of 10 mm and are subjected to 3D X-ray CT imaging (PCT-G3; 150 kV and 100 μA with CCD camera as a flat-panel detector, SEC Ltd.). The 8-bit grayscaled images are segmented to obtain the binarized pore structure by Otsu's method (Otsu, 1979) as illustrated in Figure 1a. The Jumunjin and Toyoura sands have 10.9 μm and 5.84 μm of voxel size in 300×300×300 domain and have 0.412 and 0.442 of porosity, respectively (Figure 1b).

It is well known that pore network consists of pore chambers and pore throats, and could be directly obtained from the 3D pore image. This study initially assumes the shapes of pore throats as cylindrical shapes, but simultaneously captures the pore throat's irregular cross-section to further calibrate the capillary pressure. The geometry of pore throats (Figure 1c) as well as the pore networks are obtained as follows: the skeletal network (e.g., medial axis) of 3D binary pore image is first extracted. The junctions and dead ends of pore skeleton are assigned as prospective chambers, and the remaining skeleton segments connecting two adjacent potential chambers are regarded as pore channels. A voxel along pore channel skeleton having the minimum value by Euclidean distance transform (EDT) becomes the throat center c_p and the radius of inscribed sphere r_{ins} is obtained therein. Most importantly, the virtual plane with 200×200 pixels (AA' in Figure 1c) is inserted through the predetermined c_p, perpendicular to the curve fitted to the pore skeleton. Note that the plane insertion is done by cubic interpolation to achieve sufficient resolution and to capture the irregularity of throat cross-section (e.g., 20 pixels per r_{ins}) for both LB simulation and morphological analysis (Kang et al., 2016). By assuming that pore throats have negligible volume, prospective pore chambers are fully dilated until they touch the inserted planes. This process spontaneously produces the conventional pore network structure (i.e., stick-and-ball structure) and 2D geometry of authentic pore throat cross-section.

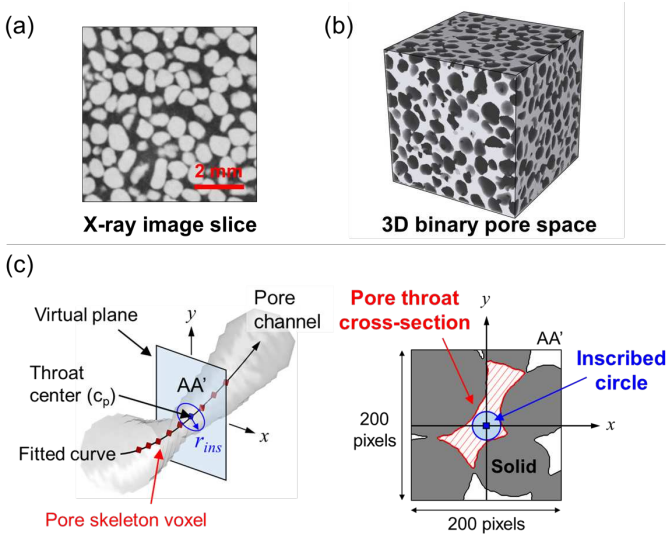

Figure 1. Extraction process of pore throat cross-sectional images and network structure. (a) 2D sliced X-ray images are binarized and then (b) stacked in 3D to construct the pore structure. (c) The virtual plane perpendicular to the pore skeleton is inserted to extract the irregularly shaped pore throat cross-section for computing capillary pressure.

2.2 *Lattice Boltzmann simulation*

The extract pore throat cross-section is first stretched out to make a 3D tube with the length of 500 pixels. The non-wetting fluid bubble with the length of 250 pixels (red colored bubble in Figure 2) is initially placed in the middle of the tube while the wetting phase fluid fills the both sides. The capillary pressure acting at the 3D tube is then numerically computed by two-phase LB bubble simulation using modified Rothman-Keller model for D3Q19 lattice proposed by Liu et al. (2012). For simplicity, we adopted the same density and viscosity conditions for both non-wetting and wetting fluids. Without any external force, the LB bubble simulation allows both non-wetting and wetting fluids to reach the equilibrium state after ~ 2×10^5 iteration steps. Then,

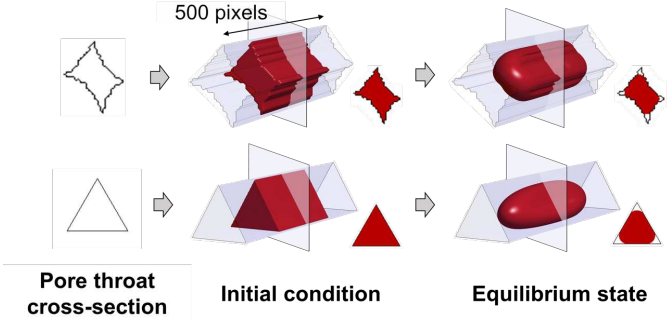

the capillary pressure p_c is measured from the differential pressure between inside and outside bubble.

Figure 2. The cross-sections of pore throats are extended to procedure 3D synthetic channel. The non-wetting bubble (red) is initially placed at the center. The LB bubble simulation allows that both wetting and non-wetting fluids reach the equilibrium state where the final configuration of both fluids are obtained.

2.3 *Morphological analysis*

Unlike polygon, for irregularly shaped pore throats, it may not be readily achievable to measure the capillary pressure and geometrical distribution of non-wetting phase fluid. Therefore, we develop the morphological analysis to identify the effective cross-section which is occupied by the non-wetting phase after drainage process (non-wetting phase fluid invading into capillary tube filled with wetting phase fluid) (Mason and Morrow, 1991). Later in this study, the effective cross-section is correlated with the capillary pressure.

The procedure starts with identifying the lower bound of the radius of the arc meniscus r_{AM}. For the fully wetting condition, the general form of Young-Laplace equation gives:

$$p_c = T_s\left(\frac{1}{r_1}+\frac{1}{r_2}\right)=\frac{T_s}{r_{AM}} \le p_{c,ins}=\frac{2T_s}{r_{ins}} \tag{1}$$

where r_1 and r_2 are the principal radii of curvature at the fluid interface, T_s is the interfacial tension, and $p_{c,ins}$ indicates the capillary pressure computed by Young-Laplace equation with $r_1 = r_2 = r_{ins}$. Here, r_{AM} is lower-bounded by half of r_{ins} and we therefore define the effective radius of curvature r_{eff} as $r_{ins}/2$ for the sake of simplicity. The effective cross-section is identified as the following (Suh et al., 2017; Suh and Yun 2017): Let $\boldsymbol{p} = (p_1, p_2, \ldots, p_m)$ and $\boldsymbol{s} = (s_1, s_2, \ldots, s_n)$ be the group of pixels of the pore and solid region in a cross-sectional image of pore throat, respectively. Then, we can first determine the zone $\boldsymbol{Z_1} \subset \boldsymbol{p}$, where Euclidean distance values from $\boldsymbol{s}$ are greater than r_{eff}:

$$\boldsymbol{Z_1} = \left\{ \boldsymbol{p}_i \mid \min_{\boldsymbol{s}_j}\left(\left\|\boldsymbol{p}_i - \boldsymbol{s}_j\right\|\right) \ge r_{eff} \ \text{ for } {}^{\forall} j \right\} \tag{2}$$

Another zone $\boldsymbol{Z_2} \subset \boldsymbol{p}$, is determined as the region where Euclidean distance values from $\boldsymbol{Z_1}$ are smaller than r_{eff}. Finally, the effective cross-section $\boldsymbol{Z_{eff}} \subset \boldsymbol{p}$ can be identified as follows:

$$\boldsymbol{Z_{eff}} = \boldsymbol{Z_1} \cup \boldsymbol{Z_2} \quad \text{where}$$

$$\boldsymbol{Z_2} = \left\{ \boldsymbol{p}_i \mid \min_{\boldsymbol{z}_j}\left(\left\|\boldsymbol{p}_i - \boldsymbol{z}_j\right\|\right) < r_{eff} \ \text{ for } \boldsymbol{z}_j \in \boldsymbol{Z_1} \right\} \tag{3}$$

The MS-P theory denotes that the capillary pressure for arbitrarily shaped flow channel is expressed by the effective area A_{eff} and perimeter P_{eff}; $p_c = T_s \cdot P_{eff}/A_{eff}$. We define the shape factor G_{eff} by utilizing the concept of the normalized capillary pressure ($p_n = p_c/p_{c,ins}$) as shown below.

$$G_{eff} = \frac{p_c}{p_{c,ins}} = \frac{T_s P_{eff}/A_{eff}}{2T_s/r_{ins}} = \frac{r_{ins}P_{eff}}{2A_{eff}} \tag{4}$$

3 RESULTS AND DISCUSSION

3.1 *Correlation between pore throat geometry and capillary pressure*

A total of 300 pore throat cross-section images (150 images from Jumunjin sand and 150 images from Toyoura sand) are subjected to the LB bubble simulation and morphological analysis. The values of normalized capillary pressure (p_n) directly computed by LB simulation and G_{eff} by morphological analysis closely run the 1:1 line with R^2 of 0.9771, regardless of the pore throat shape in Figure 3. Therefore, the capillary pressure p_c for any irregularly shaped flow channel can be readily obtained by the morphological analysis and corresponding values of G_{eff} in Eq. (4) without any additional numerical or analytical implementation as follows:

$$p_c = G_{eff}\, p_{c,ins} \tag{5}$$

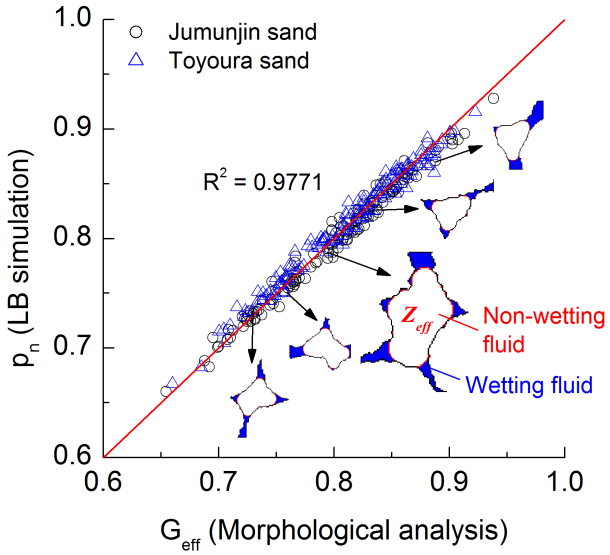

Figure 3. The relationship between the normalized capillary pressure (p_n) measured by LB simulation and the shape factors obtained by the morphological analysis (G_{eff}) with $R^2 = 0.9771$. The irregular pore throats of Jumunjin and Toyoura sands closely follows the trend line. The empty region in the cross-sectional image (effective cross-sectional area $\boldsymbol{Z_{eff}}$) is occupied by the non-wetting fluid and the blue region indicates the remaining wetting fluid.

3.2 *Water retention curve*

The iterative computation of sustained capillary pressure across the interface during drainage process allows constructing the saturation (S_w) dependent capillary pressure. And the pore-scale characteristics of such systems have been described by functional expressions for capillary pressure and wetting fluid saturation at macro-scale (Brooks and Corey, 1964; van Genuchten, 1980). We perform the pore network simulation, the method proposed by Joekar-Niasar et al. (2008), to obtain water retention curves for both Jumunjin and Toyoura sand with interfacial tension T_s of 72.8 mN/m and zero contact angle to represent the high surface energy of soil minerals (Bachmann and Van Der Ploeg, 2002; Jang and Santamarina, 2014). The obtained water retention curves are then parameterized (using air entry value p_0, fitting parameter m and residual saturation S_{wr}) by fitting the van Genuchten equation (van Genuchten, 1980):

$$p_c = p_0 \left[\left(\frac{S_w - S_{wr}}{1 - S_{wr}} \right)^{-\frac{1}{m}} - 1 \right]^{1-m} \tag{6}$$

The computed water retention curves for both sands by pore network simulation are compared with experimental data available from the literature (Tokoro et al., 2009; Ishikawa et al., 2014; Song 2014) in Figure 4.

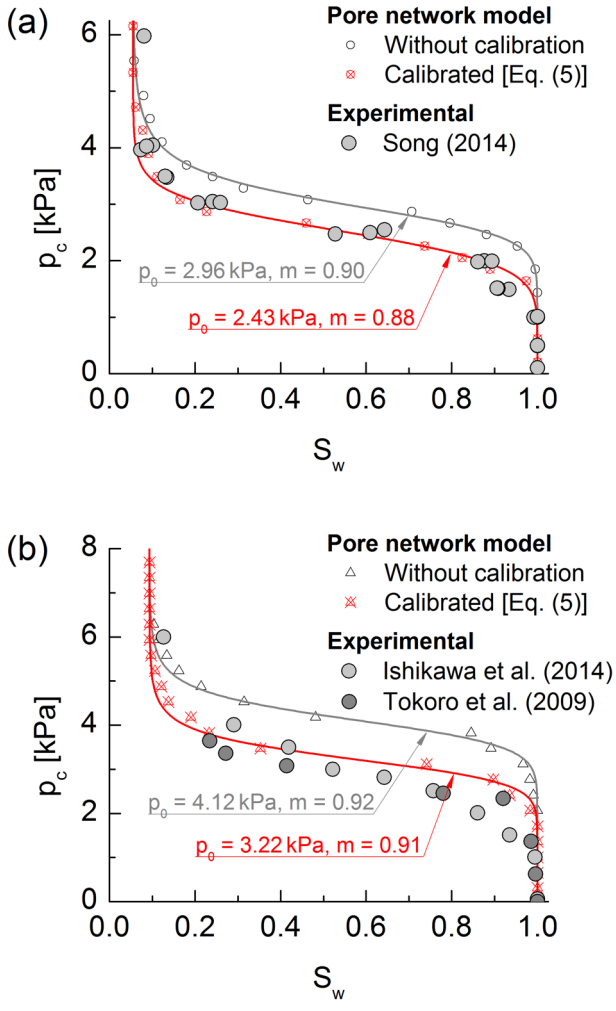

Figure 4. Water retention curves for (a) Jumunjin sand and (b) Toyoura sand. Solid lines indicate the fitted van Genuchten (1980) equation [Eq. (6)]. The experimental results (solid symbols) from the literatures (Tokoro et al., 2009; Ishikawa et al., 2014; Song 2014) strongly corroborate the evolution of capillary pressure modified by Eq. (5) (small hollow symbols) and runs below the conventional pore network simulation results (small crossed symbols) which implements inscribed circles.

The capillary pressures obtained by the conventional pore network simulation (small hollow symbols) are higher than the experimental results (solid symbols) at a given degree of saturation. Then, while the pore connectivity of the network model is maintained constant, only the capillary pressures of the tubes in the network model is calibrated by Eq. (5) considering irregularly shaped pore channels. The simulation using the calibrated pore network model results in the water retention curves (small crossed symbols) that are close to the experimental results. Based on the fitting parameters for Eq. (6), the original pore network simulation shows higher gas entry pressure and more uniform pore size distribution compared to the experimental results, however, the calibrated pore network model shows water retention characteristics very closed to experimental results. Therefore, this pore-scale simulation combined with X-ray imaging and the morphology analysis could be an alternative option to the experimental measurement of water retention curve that is costly and difficult to measure in some situations.

4 CONCLUSIONS

The capillary pressures for irregularly shaped pore throats are investigated by pore network modeling and lattice Boltzmann simulation. A relatively simple and adoptable morphological analysis to accurately compute the capillary pressure is developed by estimating its effective shape factor with the aid of MS-P theory. Pore throat cross-sections of natural sands acquired from 3D X-ray CT images are considered for investigating the validity and applicability of the proposed method. The following conclusions can be drawn:

1. 3D X-ray CT image well captures the geometrical features of real porous media, but representing pore channel by a circular tube overestimates the capillary pressure.
2. The effective shape factor enables us to obtain the capillary pressure for irregular cross-section without performing LB simulation.
3. The simulation of pore network model calibrated by the proper capillary pressures relevant to each irregular pore shape results in water retention curves similar to experimental results.

5 ACKNOWLEDGEMENTS

This work was supported by the National Research Foundation of Korea (NRF) grant funded by the Korea government (MSIP) (Nos. 2011-0030040 and 2016R1A2B4011292).

6 REFERENCES

Bachmann, J. & Van Der Ploeg, R. R. 2002. A review on recent developments in soil water retention theory: Interfacial tension and temperature effects. *Journal of Plant Nutrition and Soil Science* 165(4): 468–478.

Blunt, M. J. 2001. Flow in porous media—pore-network models and multiphase flow. *Current opinion in colloid & interface science* 6(3): 197–207.

Brooks, R. H. & Corey, A. T. 1964. Hydraulic properties of porous media and their relation to drainage design. *Transactions of the ASAE* 7(1): 26–0228.

Dong, H. & Blunt, M. J. 2009. Pore-network extraction from micro-computerized-tomography images. *Physical Review E* 80(3): 36307.

Dong, M. & Chatzis, I. 1995. The imbibition and flow of a wetting liquid along the corners of a square capillary tube. *Journal of Colloid and Interface Science* 172(2): 278–288.

Ishikawa, T., Zhang, Y., Tokora, T. & Miura, S. 2014. Medium-size triaxial apparatus for unsaturated granular subbase course materials. *Soils and Foundations* 54(1): 67–80.

Jang, J. & Santamarina, J. C. 2014. Evolution of gas saturation and relative permeability during gas production from hydrate-bearing sediments: Gas invasion vs. gas nucleation. *Journal of Geophysical Research: Solid Earth* 119(1): 116–126.

Joekar-Niasar, V. & Hassanizadeh, S. M. 2012. Analysis of Fundamentals of Two-Phase Flow in Porous Media Using Dynamic Pore-Network Models: A Review. *Critical Reviews in Environmental Science and Technology* 42(18): 1895–1976.

Joekar-Niasar, V., Hassanizadeh, S. M. & Leijnse, A. 2008. Insights into the relationships among capillary pressure, saturation, interfacial area and relative permeability using pore-network modeling. *Transport in Porous Media* 74(2): 201–219.

Kang, D. H., Yun, T. S., Kim, K. Y. & Jang, J. 2016. Effect of hydrate nucleation mechanisms and capillarity on permeability reduction in granular media. *Geophysical Research Letters* 43(17): 9018–9025.

Lago, M. & Araujo, M. 2001. Threshold Pressure in Capillaries with Polygonal Cross Section. *Journal of Colloid and Interface Science* 243(1): 219–226.

Lechman, J. & Lu, N. 2008. Capillary stress and water retention between two uneven-sized particles. *Journal of Engineering Mechanics*, 134(5): 374-384.

Likos, W. J. & Lu, N. 2004. Hysteresis of capillary cohesion in unsaturated granular soils. *Journal of Engineering Mechanics*, 130(6): 646-655.

Liu, H., Valocchi, A. J. & Kang, Q. 2012. Three-dimensional lattice Boltzmann model for immiscible two-phase flow simulations. *Physical Review E* 85(4): 1–14.

Mason, G. & Morrow, N. R. 1991. Capillary behavior of a perfectly wetting liquid in irregular triangular tubes. *Journal of Colloid and Interface Science* 141(1): 262–274.

Mayer, R. P. & Stowe, R. A. 1965. Mercury porosimetry—breakthrough pressure for penetration between packed spheres. *Journal of Colloid Science* 20(8): 893–911.

Otsu, N. 1979. A threshold selection method from gray-level histograms. *IEEE Transactions on Systems, Man, and Cybernetics* 9(1): 62–66.

Princen, H. M. 1969a. Capillary phenomena in assemblies of parallel cylinders. I. Capillary rise between two cylinders. *Journal of Colloid and Interface Science* 30(1): 69–75.

Princen, H. M. 1969b. Capillary phenomena in assemblies of parallel cylinders: II. Capillary rise between two cylinders. *Journal of Colloid and Interface Science* 30(3): 359–371.

Princen, H. M. 1970. Capillary phenomena in assemblies of parallel cylinders. III. Liquid Columns between Horizontal Parallel Cylinders. *Journal of Colloid and Interface Science* 34(2): 171–184.

Ramstad, T., Oren, P. E. & Bakke, S. 2009. Simulation of Two Phase Flow in Reservoir Rocks Using a Lattice Boltzmann Method, *SPE Annual Technical Conference and Exhibition*.

Raoof, A., Nick, H. M., Hassanizadeh, S. M. & Spiers, C. J. 2013. PoreFlow: A complex porenetwork model for simulation of reactive transport in variably saturated porous media *Computers and Geosciences* 61: 160–174.

Silin, D. & Patzek, T. 2006. Pore space morphology analysis using maximal inscribed spheres. *Physica A: Statistical Mechanics and its Applications* 371(2): 336–360.

Song, Y. S. 2014. Suction stress in unsaturated sand at different relative densities, *Engineering Geology* 176: 1–10.

Suh, H. S., Kang, D. H., Jang, J., Kim, K. Y. & Yun, T. S. 2017. Capillary pressure at irregularly shaped pore throats: Implications for water retention characteristics. *Advances in Water Resources*.

Suh, H. S. & Yun, T. S. 2017. Modification of capillary pressure by considering pore throat geometry with the effects of particle shape and packing features on water retention curves for uniformly graded sands. *Computers and Geotechnics*.

Tokoro, T., Ishikawa, T. & Miura, S. 2009. Effect of cross section of plumbing path on coefficient of permeability of unsaturated sand. *In Proceedings of the 44th annual conference on Japan Society of Civil Engineers*, 936–944.

van Genuchten, M. T. 1980. A Closed-form Equation for Predicting the Hydraulic Conductivity of Unsaturated Soils. *Soil Science Society of America Journal* 44(5): 892.

Wilson, C., Lu, N. & Likos, W. J. 2012. Quantification of Grain, Pore, and Fluid Microstructure of Unsaturated Sand from X-Ray Computed Tomography Images, *Geotechnical Testing Journal*, 35(6): 911-923.

Yang, F., Hingerl, F. F., Xiao, X., Liu, Y., Wu, Z., Benson, S. M. & Toney, M. F. 2015. Extraction of pore-morphology and capillary pressure curves of porous media from synchrotron-based tomography data. *Scientific reports* 5.